HHS Public Access

Author manuscript

Conf Proc IEEE Eng Med Biol Soc. Author manuscript; available in PMC 2020 July 01.

Published in final edited form as:

Conf Proc IEEE Eng Med Biol Soc. 2019 July ; 2019: 2336–2339. doi:10.1109/EMBC.2019.8857384.

Source localization for gastric electrical activity using simulated magnetogastrographic data

Recep Avci[1], **Niranchan Paskaranandavadivel**[1], **Stefan Calder**[1], **Peng Du**[1], **Leonard A. Bradshaw**[2], **Leo K. Cheng**[1,2]

[1]Auckland Bioengineering Institute, University of Auckland, Auckland, New Zealand. [2]Department of Surgery, Vanderbilt University, Nashville, Tennessee, USA.

Abstract

In this study, we investigated the use of magnetic dipole (MDP) approximation to localize the underlying source of magnetogastrographic (MGG) data. An anatomically realistic torso and a stomach model were used to simulate slow wave (SW) activities and magnetic fields (MFS). SW activation in the stomach was simulated using a grid-based finite element method. The SW activity of the stomach at each time sample was represented by the dipoles generated for each element and MFs were computed from these dipoles including secondary sources in the torso. Gaussian noise was added to the MFs to represent experimental signal noise. Then, MDP fitting was executed on the time samples of selected 2-second time frames. For each sample, goodness of fit (GOF) and the distance from the fitted MDP to the center of gravity (COG) of active dipoles were computed. Then, for each time frame, we analyzed the spatial changes of COG and MDP positions in x-, y-, and z-directions and computed correlation scores. Our results showed that MDP fitting was capable of identifying propagation patterns with mean correlation scores of 0.63±0.30, 0.71±0.19, and 0.81 ± 0.24 in x-, y-, and z-directions, respectively. The mean distance from COGs to the identified MDPs was 49 ± 4 mm. The results were similar under the noise conditions as well. Our results suggest that source localization using MDP approximation can be useful to identify the propagation characteristics of SWs using MGG.

I. Introduction

Rhythmic and coordinated gastric electrical activities known as slow waves (SWs) are responsible for the contractions of gastrointestinal (GI) organs [1]. GI motility disorders are associated with abnormal SW activities in the gut [2], [3]. Some of these abnormalities include spatially-complex dysrhythmias which occur within the normal SW frequency range [4]. Monitoring and identifying these abnormal SW activities is important to diagnose and understand the underlying reasons of gastric disorders.

High resolution mapping of SW activities [5], [6] enables to analyze SW activation and propagation in spatiotemporal detail but the invasiveness limits its clinical utility as a routine diagnostic method. Non-invasive electrogastrography (EGG) measurements using cutaneous

recep.avci@auckland.ac.nz.

electrodes [7], [8] are also capable of capturing SW activity to some extent, but the electrical resistance of body tissues compromises the measurement of gastric currents with low amplitudes. It has been also shown that the magnetic fields (MFs) generated by the gastric electric activity known as magnetogastrography (MGG) can be reliably recorded as well using superconducting quantum interference device (SQUID) arrays [9]. The MGG signals are attenuated less by the muscle and fat layers in the abdominal wall than EGG signals.

A more comprehensive understanding of the relationship between SWs and these non-invasive measurements is needed to identify the abnormal SW activities. Analyzing source dynamics and monitoring the changes in the source domain can be informative in this regard. Several studies have previously focused on analyzing source dynamics using simulated or real EGG and MGG data [10], [11], [12]. One major challenge in source-based analyses is that the models are generally dependent on the volume conductor.

Previous cardiac studies showed that biomagnetic fields measured outside the body can be described as the field of a magnetic dipole (MDP) moment [13], [14]. Moreover, the identified dipole moments and positions are shown to be directly related with the depolarization of cardiac tissues [14]. The advantage of MDP model is that its physical definition is independent from the volume conductor. It can sufficiently explain the measured biomagnetic data since the higher-order components of MFs are not usually observed as they drop-off with distance more rapidly [15].

In this study, we have investigated the use of MDP moment in source localization of gastric electrical activity using simulated SW and MGG data.

II. Methods

A. Simulations

Gastric SWs and MFs were simulated using anatomically realistic stomach and torso models constructed from CT images. The stomach and torso geometries were converted to 3D data cloud and were defined by 256 and 4178 elements, respectively. SW activation in the stomach was simulated using a grid-based finite element method similar to a previous study [16]. We simulated two SW propagation patterns e.g., antegrade and retrograde from two different pacemaker locations. The SW activity of the stomach at each time sample was represented by the dipoles generated for each element based on the simulated membrane potentials and conductivities. Depending on the locations of the SWs, only dipoles in the elements with existing SWs were active i.e., the majority of the dipoles had negligible sizes. Using these active dipoles as primary sources and the realistic torso model as the volume conductor, MF gradients in the y-direction were computed on a hypothetical high-density SQUID array where the 176 sensors were 20 mm distant from each other. Simulations were performed with a sampling frequency of0.1 Hz using CMISS [17].

B. Source Localization

1) Forward Model: Let $\boldsymbol{B} = [\boldsymbol{b}_1, \ldots, \boldsymbol{b}_N]$ be the set of MFs on N sensors. Then, $\boldsymbol{B}$ can be expressed as a linear combination of an MDP moment $\boldsymbol{m}$ located at $\boldsymbol{r}_m$ and a gain matrix $\boldsymbol{G}$ as follows: $\boldsymbol{B} = \boldsymbol{G}\boldsymbol{m}$. The matrix representation of $\boldsymbol{B}$ reduces the computational complexity

of the source localization by separating the linear moment parameters from the location parameters [18]. The matrix representation of MFs due to the MDP moment was studied in [19]. The matrix $\boldsymbol{G}$ is a function of the sensor location and dipole position. It is composed of kernel matrices of sensors i.e., $\boldsymbol{G} = [\boldsymbol{v}_1 \cdot \boldsymbol{K}_1, \ldots, \boldsymbol{v}_N \boldsymbol{K}_N]^T$ where $\boldsymbol{v}_i$ is the direction vector between two coils in the gradiometers and T is the transpose operator. The kernel matrix, $\boldsymbol{K}_i$ for the i-th sensor located at $\boldsymbol{r}_i$ can be computed as follows:

$$\boldsymbol{K}_i = \frac{\mu_0}{4\pi}\left(\frac{3\left(\boldsymbol{d}_i \boldsymbol{d}_i^T\right)\boldsymbol{I}}{d_i^5} - \frac{\boldsymbol{I}}{d_i^3}\right), \tag{1}$$

where μ_0 is the permeability constant, $\boldsymbol{d}_i = \boldsymbol{r}_i - \boldsymbol{r}_m$, and $\boldsymbol{I}$ is an identity matrix.

2) Inverse Solution: Estimating MDP moment and its position from a set of MFs under white noise can be considered as a general problem of estimating these parameters from a Gaussian model. For $\boldsymbol{B}$, unbiased estimates of $\boldsymbol{r}_m$ and $\boldsymbol{m}$ (denoted as $\hat{\boldsymbol{r}}_m$ and $\hat{\boldsymbol{m}}$, respectively) can be obtained using maximum likelihood estimate (MLE) [20] by minimizing the following function:

$$F(\boldsymbol{r}_m) = \mathrm{tr}\left\{\left(\boldsymbol{I} - \boldsymbol{G}\left(\boldsymbol{G}^T\boldsymbol{G}\right)^{-1}\boldsymbol{G}^T\right)\hat{R}\right\}, \tag{2}$$

where $\mathrm{tr}\{\cdot\}$ is the trace operator and $\hat{R}$ is an estimate of the covariance matrix obtained from $\boldsymbol{B}$. Then, $\hat{\boldsymbol{r}}_m$ is given by the following formula:

$$\hat{\boldsymbol{r}}_m = arg\left\{\min_{\boldsymbol{r}_m} F(\boldsymbol{r}_m)\right\}. \tag{3}$$

After $\hat{\boldsymbol{r}}_m$ is estimated, the dipole moment can be obtained by a simple least-squares fit, i.e.,

$$\hat{\boldsymbol{m}} = \left(\hat{\boldsymbol{G}}^T\hat{\boldsymbol{G}}\right)^{-1}\hat{\boldsymbol{G}}^T\boldsymbol{B}, \tag{4}$$

where $\hat{\boldsymbol{G}}$ is the gain matrix due to the position $\hat{\boldsymbol{r}}_m$. Then, $\hat{\boldsymbol{B}}$ can be forward-computed using $\hat{\boldsymbol{m}}$ and $\hat{\boldsymbol{r}}_m$.

C. Comparison Metrics

The performance of source localization was evaluated using the goodness of fit (GOF):

$$GOF = 1 - \frac{\|\boldsymbol{B} - \hat{\boldsymbol{B}}\|_2}{\|\boldsymbol{B}\|_2} \tag{5}$$

where $\|\cdot\|_2$ is the Euclidean norm.

Since moving multiple dipoles are responsible for generating the MFs, the location and propagation pattern of the fitted MDPs were compared with the center of gravity (COG) of active dipoles where COG was computed as follows:

$$COG = \frac{\sum_{i=1}^{n} \left(|q_x^i| r_x^i, |q_y^i| r_y^i, |q_z^i| r_z^i \right)}{\sum_{i=1}^{n} \left(|q_x^i|, |q_y^i|, |q_z^i| \right)}, \quad (6)$$

where $\boldsymbol{q} = (q_x^i, q_y^i, q_z^i)$ is the i-th active dipole, r_x^i, r_y^i, and r_z^i are the coordinates of its position. We computed the distance between the COG and the fitted MDP positions for each time sample and the correlation of spatial changes observed in x-, y-, and z-directions for a period of 2 seconds.

III. Results

Fig. 1(A) displays the torso and stomach geometries used in our simulations together with the sensor positions. Our simulations generated both antegrade and retrograde SW activities on the stomach. Based on the frequency of activation, there were some time periods where we observed only one single SW activity or two different SWs on the stomach. In other words, MFs were generated by the active dipoles of either one or two SW activities. The simulation results of the transmembrane potential solution on the stomach at one time point for antegrade propagation are shown in Fig. 1(B–C). The figures show an example of both the single and double SW activities together with their corresponding active dipoles.

We visually inspected SW propagations and selected three different 2-second time frames from both antegrade and retrograde simulations. In the first two time frames, there existed only one SW activity located on either mid-corpus or antrum. In the third time frame, there were two SW activities, one on the corpus and one on the antrum. For each of these time frames, we performed source localizations for 20 samples independently. No temporal information was included in the source localization process.

Fig. 2 displays the source localization results for the time frame where a single antegrade SW activity was observed. In Fig. 2(A) the SW activity for the tenth time sample is shown while its resultant MF activity on SQUID sensors can be seen in Fig. 2(D). Ten of the identified MDP positions (every other starting from the first one) were plotted with small spheres in Fig. 2(B–C), where the green sphere corresponds to the first time sample. Even though the identified dipole positions are high off the stomach, they follow a similar pattern as SW propagated. Fig. 2(E) displays the MF computed from the identified MDP moment for the tenth time sample. As seen in Fig. 2(D–E), the MF distribution over the sensors were very similar and the GOF value for this time sample was 91%.

When there were two active SWs, the best-fitted MDPs were located between the active dipoles of two SWs following a similar propagation pattern. Fig. 3 displays a retrograde propagation with two SW activities. The blue spheres correspond to the positions of every other fitted MDP. As seen in Fig. 3, the fitted dipoles are between the two SW activities and propagating towards the fundus. The green spheres display the fitted MDP positions for each time point shown in the figures. Note that the MDP positions are also moving towards the lesser curvature as the SW activity on the antrum propagates circumferentially.

We performed source localization under noise conditions as well. We first added uncorrelated random noise distributed as $\mathcal{N}(0, \sigma^2)$ to produce mean signal-to-noise ratio (SNR) of 20 and 10 dB. Then, we executed source localization using these noise-added data sets and estimated the MDP positions. Due to the randomization in the noise adding process, this procedure was repeated 30 times for both the SNRs of 20 and 10 dB. The comparison and performance metrics e.g., GOF values, the distance, the velocity, and correlation scores were computed at each run and each metric was represented by the mean value of 30 runs. Table I shows descriptive statistics of these metrics for both noiseless and noise-added cases. The SNR of 10 dB resulted lower GOF values and for most of the data sets source localization resulted a GOF value over 80% for the SNR of 20 dB. Other metrics did not show significant changes under the noise conditions.

IV. Discussion

The use of MDP fitting in source localization of MGG data was investigated in this study. The MGG data was generated by multiple dipoles representing the SW activity of the stomach. In general we obtained high GOF values suggesting that the best fitted MDP described the majority of the MGG data. Even though having high GOF values usually implies better source localization performance, the inverse solutions are known to be ill-posed and cannot be uniquely solved, because the same field distribution can be produced by other source configurations as well [21].

It is important to test the sensitivity of MDP approximation to different SW propagation patterns. Therefore, both antegrade and retrograde SWs were simulated and resultant MFs were computed. We have shown that MDP approximation was informative about the propagation direction. In general, the correlation scores for the directions where the COG of active dipoles significantly moved were higher. There were some time frames in which the COG did not change a lot in certain directions and low correlation scores were noted.

Our results suggest that MDP fitting is capable of identifying propagation patterns with the mean correlation scores of 0.63 ± 0.3, 0.71 ± 0.2, and 0.81 ± 0.2 in x-, y-, and z-directions, respectively. Note that these mean correlations were obtained by averaging the correlation scores of all selected time frames and the major propagation direction was varying among these time frames. We have demonstrated that the spatial changes in active dipoles and the identified MDP positions are correlated and MDP approximation can provide insight about the propagation patterns of SWs.

Distances from localized MDP positions to COGs of active dipoles were about 4 cm but there were some time frames producing over 10 cm distances as well. Since we have multiple active dipoles at each time sample and these dipoles are distributed around stomach tissues, the distances obtained were within error limits. Another important point is that our MF calculations included secondary sources as well but the the positions of MDP were compared with the primary sources i.e., active dipoles representing SW activities.

When two SWs activities were present on the stomach, MDPs were fitted between two SWs. Therefore, MDP fitting yielded more accurate localization results when a single SW was

present. Yet, the MDP fitting provided conclusive and accurate results about the propagation patterns in both cases. This is significant because normal SW activity usually has a frequency of 3 cpm [22] and it is very unlikely to have a single SW activity on the stomach.

Interestingly adding noise to the MGG data did not have a considerable effect on source localization performance other than a decrease in the GOF values which was a natural consequence of noise addition. Considering the amount of noise we have added, we can say that MDP fitting seems robust under the noise conditions and provides accurate results.

One limitation in this study is that we have not tested MDP fitting on experimental MGG measurements. Even though we have used realistic stomach and torso geometries, further studies on experimental MGG data are needed to validate our results. Simulating more complex propagation patterns and using different torso and stomach geometries will be the other future direction of this study.

V. Conclusion

This study demonstrates the use of magnetic dipole approximation in source localization of MGG data. Our results showed that MDP fitting provides a robust and informative way to investigate the propagation dynamics of slow wave activities in the stomach. In the future, the optimized version of this method has a potential to be a useful means in diagnosis of electrical dysrhythmias in the gastrointestinal system.

Acknowledgments

Research supported by Health Research Council of NZ, the Marsden Fund Council of NZ, and NIH (R01 HD 088662)

References

[1]. Szurszewski J, “A 100-year perspective on gastrointestinal motility,” Am. J. Physiol. Gastrointest. Liver Physiol, vol. 274, no. 3, pp. G447–G453, 1998.

[2]. Lammers WJ, Ver Donck L, Stephen B, Smets D, and Schuurkes JA, “Focal activities and re-entrant propagations as mechanisms of gastric tachyarrhythmias,” Gastroenterology, vol. 135, no. 5, pp. 1601–1611, 2008. [PubMed: 18713627]

[3]. O’Grady G, Wang TH-H, Du P, Angeli T, Lammers WJ, and Cheng LK, “Recent progress in gastric arrhythmia: pathophysiology, clinical significance and future horizons,” Clin. Exp. Pharmacol. Physiol, vol. 41, no. 10, pp. 854–862, 2014. [PubMed: 25115692]

[4]. Du P, Calder S, Angeli TR, Sathar S, Paskaranandavadivel N, O’Grady G, and Cheng LK, “Progress in mathematical modeling of gastrointestinal slow wave abnormalities,” Front. Physiol, vol. 8, p. 1136, 2018.

[5]. Lammers W, Stephen B, Arafat K, and Manefield G, “High resolution electrical mapping in the gastrointestinal system: initial results,” J. Neurogastroenterol. Motil, vol. 8, no. 3, pp. 207–216, 1996.

[6]. Du P, O’Grady G, Egbuji J, Lammers W, Budgett D, Nielsen P, Windsor J, Pullan A, and Cheng L, “High-resolution mapping of in vivo gastrointestinal slow wave activity using flexible printed circuit board electrodes: methodology and validation,” Ann. Biomed. Eng, vol. 37, no. 4, p. 839, 2009. [PubMed: 19224368]

[7]. Familoni B, Kingma Y, and Bowes K, “Study of transcutaneous and intraluminal measurement of gastric electrical activity in humans,” Med. Biol. Eng. Comput, vol. 25, no. 4, pp. 397–402, 1987. [PubMed: 3450990]

[8]. Lin X and Chen JZ, “Abnormal gastric slow waves in patients with functional dyspepsia assessed by multichannel electrogastrography,” Am. J. Physiol. Gastrointest. Liver Physiol, vol. 280, no. 6, pp. G1370–G1375, 2001. [PubMed: 11352832]

[9]. Bradshaw L, Irimia A, Sims J, Gallucci M, Palmer R, and Richards W, “Biomagnetic characterization of spatiotemporal parameters of the gastric slow wave,” J. Neurogastroenterol. Motil, vol. 18, no. 8, pp. 619–631, 2006.

[10]. Allescher H, Abraham-Fuchs K, Dunkel R, and Classen M, “Biomagnetic 3-dimensional spatial and temporal characterization of electrical activity of human stomach,” Dig. Dis. Sci, vol. 43, no. 4, pp. 683–693, 1998. [PubMed: 9558020]

[11]. Bradshaw LA, Cheng LK, Richards WO, and Pullan AJ, “Surface current density mapping for identification of gastric slow wave propagation,” IEEE Trans. Biomed. Eng, vol. 56, no. 8, pp. 2131–2139, 2009. [PubMed: 19403355]

[12]. Kim J, Du P, and Cheng L, “Reconstruction of normal and abnormal gastric electrical sources using a potential based inverse method,” Physiol. Meas, vol. 34, no. 9, p. 1193, 2013. [PubMed: 24137714]

[13]. Brockmeier K, Schmitz L, Bobadilla-Chavez JD, Burghoff M, Koch H, Zimmermann R, and Trahms L, “Magnetocardiography and 32-lead potential mapping: Repolarization in normal subjects during pharmacologically induced stress,” J. Cardiovasc. Electrophysiol, vol. 8, no. 6, pp. 615–626, 1997. [PubMed: 9209962]

[14]. Avci R, Wilson JD, Escalona-Vargas D, and Eswaran H, “Tracking fetal movement through source localization from multisensor magnetocardiographic recordings,” IEEE J. Biomed. Health. Inform, vol. 22, no. 3, pp. 758–765, 2018. [PubMed: 28391212]

[15]. Malmivuo J and Plonsey R, Bioelectromagnetism: Principles and Applications of Bioelectric and Biomagnetic Fields, 1st ed. Oxford University Press, USA, 1995.

[16]. Calder S, O’Grady G, Cheng LK, and Du P, “A theoretical analysis of electrogastrography (EGG) signatures associated with gastric dysrhythmias,” IEEE Trans. Biomed. Eng, vol. 64, no. 7, pp. 1592–1601, 2017. [PubMed: 28113227]

[17]. CMISS: An interactive computer program for continuum mechanics, image analysis, signal processing and system identification. [Online]. Available: http://www.cmiss.org

[18]. Mosher JC, Leahy RM, and Lewis PS, “EEG and MEG: forward solutions for inverse methods,” IEEE. Trans. Biomed. Eng, vol. 46, no. 3, pp. 245–259, 3 1999. [PubMed: 10097460]

[19]. Avci R, “Inverse and forward solutions on fetal magnetocardiography: Hybrid dipole model,” Ph.D. dissertation, University of Arkansas at Little Rock, 2017.

[20]. Stoica P and Nehorai A, “Music, maximum likelihood, and cramer-rao bound,” IEEE Trans. Acoust., Speech, Signal Processing, vol. 37, no. 5, pp. 720–741, 1989.

[21]. Vrba J, Robinson SE, McCubbin J, Lowery CL, Eswaran H, Murphy P, and Preissl H, “Searching for the best model: ambiguity of inverse solutions and application to fetal magnetoencephalography,” Phys. Med. Biol, vol. 52, no. 3, p. 757, 2007. [PubMed: 17228119]

[22]. Cheng LK, O’Grady G, Du P, Egbuji JU, Windsor JA, and Pullan AJ, “Gastrointestinal system,” Wiley Interdiscip. Rev. Syst. Biol. Med, vol. 2, no. 1, pp. 65–79, 2010. [PubMed: 20836011]

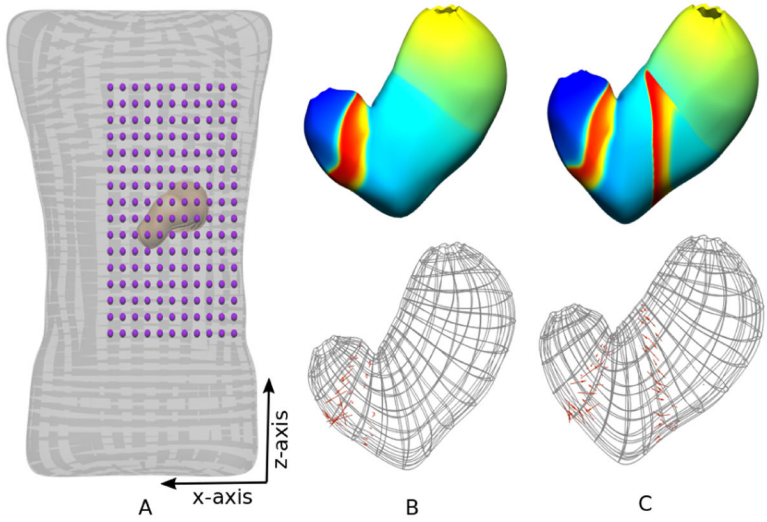

Fig. 1.

A) Stomach and torso geometry used in simulations together with the SQUID sensors. B-C) Transmembrane potentials of single and double SW activity (top) and their corresponding active dipoles shown as red arrows (bottom).

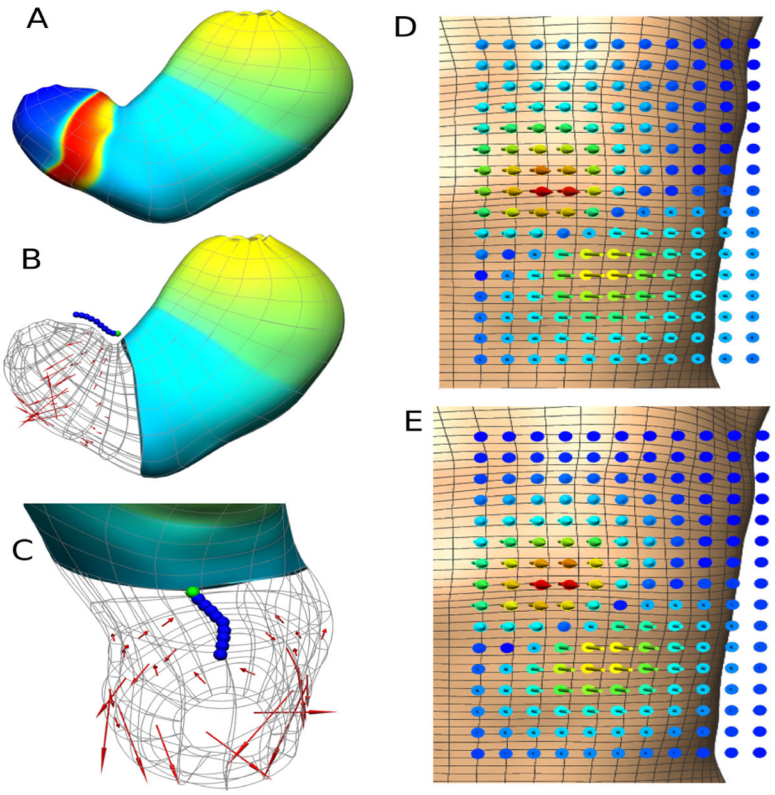

Fig. 2.

A) Transmembrane potential for a single SW in the tenth time sample of the selected time frame. B-C) Two different views of the active dipoles representing the SW activity and the MDP positions (small spheres) identified in the source localization. D) The MF gradient generated by the SW activity of stomach for the tenth time sample. E) The forward-computed MF gradient using the identified magnetic dipole moment for the tenth time sample.

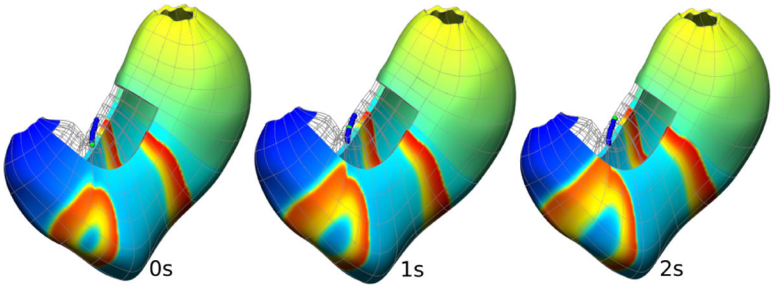

Fig. 3.

MDP fitting for two SW activities. The green sphere corresponds to the fitted MDP position of the SW activity shown in the figures. Some elements in the lesser curvature were hidden to show the MDP positions.

TABLE I

Descriptive statistics of comparison and performance metrics. Data are represented as mean ± SD.

	Noiseless	SNR20	SNR10
GOF (%)	88.3 ± 0.6	83.8 ± 1.3	65.6 ± 0.8
Distance (mm)	48.8 ± 3.9	49.0 ± 3.6	49.1 ± 3.7
Velocity (mm/s)	11.2 ± 1.9	10.0 ± 3.5	10.0 ± 3.1
Correlation X	0.63 ± 0.3	0.61 ± 0.3	0.50 ± 0.3
Correlation Y	0.71 ± 0.2	0.69 ± 0.2	0.58 ± 0.1
Correlation Z	0.81 ± 0.2	0.79 ± 0.2	0.70 ± 0.2